Femtosecond quantum interference control of electrical currents in GaAs: Signatures beyond the perturbative $\chi^{(3)}$ limit

E. Sternemann,[1] T. Jostmeier,[1] C. Ruppert,[1] H. T. Duc,[2,3] T. Meier,[2] and M. Betz[1,*]

[1]*Experimentelle Physik 2, TU Dortmund, Otto-Hahn-Straße 4, 44227 Dortmund, Germany*

[2]*Department of Physics and CeOPP, Universität Paderborn, Warburger Straße 100, 33098 Paderborn, Germany*

[3]*Ho Chi Minh City Institute of Physics, Vietnam Academy of Science and Technology, Mac Dinh Chi Street 1, District 1, Ho Chi Minh City, Vietnam*

(Received 1 September 2013; published 21 October 2013)

We present a comprehensive experimental and theoretical study of the power dependence of coherently controlled currents in bulk GaAs. Currents are optically induced by phase-stable femtosecond $\omega/2\omega$ pulse pairs. For moderate irradiances, these currents are linked to the third-order optical nonlinearity $\chi^{(3)}(0;\omega,\omega,-2\omega)$. Here we focus on elevated irradiances where absorption saturation and ultimately the onset of Rabi oscillations contribute to the optical response. Current diagnostics is achieved electrically by recording the photoresponse of contacted specimens of low temperature grown GaAs as a function of the relative phase of the ω and 2ω pulses. For stronger ω irradiance we find the magnitude of the coherently controlled current to be markedly reduced when compared to the $\chi^{(3)}$ expectation $dJ/dt \propto E_\omega^2 E_{2\omega}$. Additional pump-probe type experiments corroborate that this current saturation is indeed predominantly linked to macroscopic band filling. Theoretical simulations for the coherently controlled current based on a 14 band $\mathbf{k}\cdot\mathbf{p}$ model agree well with the experimental trends.

DOI: 10.1103/PhysRevB.88.165204 PACS number(s): 78.47.jh

I. INTRODUCTION

Current flow through semiconductor devices is usually achieved by applying potential differences to contacts. Over the last 15 years, however, all-optical concepts to induce charge transport have sparked the interest of researchers. Such techniques are particularly appealing because currents can be located wherever one can focus an optical beam. In addition, the use of femtosecond pulses provides a THz bandwidth for current control—something contact-based methods cannot do. Depending on the symmetry of the material, different nonlinear optical configurations can be utilized to induce electrical currents as well as pure spin currents. In noncentrosymmetric media such as GaAs, currents can be injected via a second-order nonlinearity. Referred to as circular photogalvanic effect[1,2] or shift current,[3] it is related to a minute shift of the charge distribution within the unit cell during the optical excitation. Larger current flows can be induced by phase-stable superpositions of a fundamental beam (ω) and its second harmonic (2ω).[4,5] In cubic semiconductors, this process is related to a third-order optical nonlinearity ($\chi^{(3)}$) and arises from a quantum interference of one- and two-photon absorption pathways across the direct gap E_G of a semiconductor which satisfies $\hbar\omega < E_G < 2\hbar\omega$. In essence this current injection directly prepares an asymmetric carrier distribution in k space and gives, thereby, rise to a macroscopic current subject to subsequent momentum relaxation. The process has been established in the prototypical material GaAs and subsequently applied to two-dimensional systems, indirect semiconductors as well as nanostructures.[6,7]

In practically all these experiments a current scaling $dJ/dt \propto E_\omega^2 E_{2\omega} \sin(2\phi_\omega - \phi_{2\omega})$ was found, where E and ϕ denotes the electric field amplitude and the phases of the pulses, respectively. Such a scaling is characteristic of a $\chi^{(3)}(0,\omega,\omega,-2\omega)$ description of current injection. In some studies, slight deviations were identified for elevated 2ω illumination and related to an internal discharge of the photoinduced electron-hole dipole.[8,9] However, for the conceptually similar injection of pure spin currents where dielectric relaxation does not occur, even a detailed experimental analysis did not reveal departures from the established $\chi^{(3)}$ picture.[10] Theoretical results, instead, suggest that strong irradiance with either ω or 2ω pulses should reveal marked departures from the perturbative $\chi^{(3)}$ scaling.[11–13] Those deviations are related to macroscopic state filling during the interaction with femtosecond light pulses. Ultimately, the simulations even predict weak signatures of Rabi flops occurring at the interband transition. While the field strengths required to achieve such strong excitation conditions are within easy reach of modern femtosecond optical sources, this limit remains experimentally unexplored to date.

The purpose of the present article is a careful experimental and theoretical analysis of room-temperature current injection in GaAs in order to explore departures of current injection from the perturbative $\chi^{(3)}$ limit. It is organized as follows: Section II lays out the theoretical work based on a 14-band $\mathbf{k}\cdot\mathbf{p}$ model for GaAs and the interaction with optical pulses as used in the experiment. The simulation results for elevated irradiances predict current injection to deviate markedly from the perturbative $\chi^{(3)}$ picture. The experimental setup is described in Sec. III. Currents are induced with tightly focused $\omega/2\omega$ pulse pairs derived from a femtosecond Er:fiber source and characterized by electrical contacts attached to mesoscopic GaAs specimens. Section IV A shows the experimental results for the coherently controlled photocurrents as a function of ω and 2ω irradiances and compares them to the simulation. For elevated excitation levels we clearly identify pronounced reductions of the current magnitude when compared to the $\chi^{(3)}$ expectation. In the remainder of Sec. IV, we present additional experimental checks to confirm that the current saturation observed in the experiment is indeed related to absorption saturation as well as band filling and only in part to

an internal discharge of the photoinjected electron-hole dipole. Those results are particularly helpful in putting our results into perspective to previous reports on apparent departures from the perturbative $\chi^{(3)}$ picture[8,9] which are indeed well described by dielectric discharge of the photoinduced electric dipole rather than revealing novel aspects of the coherent control process.

II. THEORETICAL MODEL AND SIMULATION RESULTS

We follow the theoretical approach described in Ref. 13. In short, we analyze the dynamical optoelectronic response using the multiband semiconductor Bloch equations (SBE)[13]

$$-i\hbar\left(\frac{\partial}{\partial t}x_{\mathbf{k}}^{\lambda\lambda'}-\frac{\partial}{\partial t}\,x_{\mathbf{k}}^{\lambda\lambda'}\Big|_{\text{coll}}\right)=\left(\epsilon_{\mathbf{k}}^{\lambda}-\epsilon_{\mathbf{k}}^{\lambda'}\right)x_{\mathbf{k}}^{\lambda\lambda'}+\frac{e\mathbf{A}(t)}{m_0}\cdot\sum_{\mu}\left[\mathbf{\Pi}_{\mathbf{k}}^{\mu\lambda}x_{\mathbf{k}}^{\mu\lambda'}-\mathbf{\Pi}_{\mathbf{k}}^{\lambda'\mu}x_{\mathbf{k}}^{\lambda\mu}\right],\tag{1}$$

where $x_{\mathbf{k}}^{\lambda\lambda}\equiv n_{\mathbf{k}}^{\lambda}$ is the population of electron with wave vector $\mathbf{k}$ in the band λ and $x_{\mathbf{k}}^{\lambda\lambda'}$ with $\lambda\neq\lambda'$ is the coherence between two bands λ and λ'. The collision term $\frac{\partial}{\partial t}x_{\mathbf{k}}^{\lambda\lambda'}|_{\text{coll}}$ describes either the relaxation of population or the dephasing of coherence. Here, we treat this term in a phenomenological approach. We assume that the relaxation towards the quasiequilibrium Fermi-Dirac distributions $n_{\text{FD}}^{\lambda}(\mathbf{k},T)$ is given by $\frac{\partial}{\partial t}n_{\mathbf{k}}^{\lambda}|_{\text{coll}}=-[n_{\mathbf{k}}^{\lambda}-n_{\text{FD}}^{\lambda}(\mathbf{k},T)]/\tau_1$ and the dephasing is described by $\frac{\partial}{\partial t}x_{\mathbf{k}}^{\lambda\lambda'}|_{\text{coll}}=-x_{\mathbf{k}}^{\lambda\lambda'}/\tau_2$. In the calculation we use a typical value of 150 fs for both relaxation time τ_1 and dephasing time τ_2. In order to obtain the realistic band energy $\epsilon_{\mathbf{k}}^{\lambda}$ and momentum matrix elements $\mathbf{\Pi}_{\mathbf{k}}^{\lambda\lambda'}$ in Eq. (1), we employ a 14-band $\mathbf{k}\cdot\mathbf{p}$ theory[14] with room-temperature parameters for GaAs. The vector potential $\mathbf{A}$ in Eq. (1) is given by $\mathbf{A}(t)=-\int_{-\infty}^{t}\mathbf{E}(t)dt$, where $\mathbf{E}(t)$ is the electric field of laser pulses. For the optical excitation of two collinearly polarized ω and 2ω pulses, the field takes the form

$$E(t)=E_{\omega}e^{-(t^2/2\tau_L^2)}\cos(\omega t+\phi_{\omega})+E_{2\omega}e^{-(t^2/2\tau_L^2)}\cos(2\omega t+\phi_{2\omega}).\tag{2}$$

Since we consider the optical excitation with energies far above the excitonic levels, the contribution of excitonic effects would be small and has been neglected in our calculations.

The population obtained from the SBE is used to evaluate the time-dependent current density

$$\mathbf{J}(t)=\frac{e}{m_0}\sum_{\lambda,\mathbf{k}}\mathbf{\Pi}_{\mathbf{k}}^{\lambda\lambda}n_{\mathbf{k}}^{\lambda}.\tag{3}$$

We calculate the current density in GaAs bulk which is excited by Gaussian $\omega/2\omega$ pulses with $\tau_L=100$ fs and $2\hbar\omega=1.6$ eV. The phase relation $\phi_{2\omega}-2\phi_{\omega}=\pi/2$ is chosen in order to maximize the current. The dependence of the calculated current density on the amplitude of the electric field E_{ω} for fixed $E_{2\omega}$ amplitudes is shown in Fig. 1.

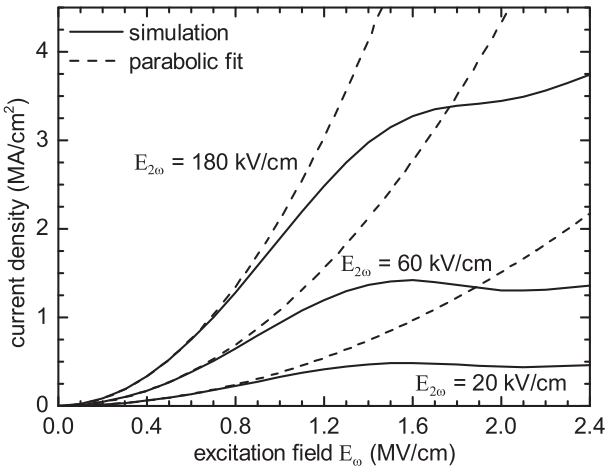

FIG. 1. Simulated dependence on the E_{ω} amplitude for fixed $E_{2\omega}$ amplitudes of current density at 100 fs after the pulse maximum. Here, incident pulses have a duration of $\tau_L=100$ fs, the 2ω pulse has photon energy of 1.6 eV, and the temperature is $T=300$ K. The parabolic fits correspond to the perturbative $\chi^{(3)}$ model.

III. EXPERIMENTAL SETUP AND SAMPLES

The scheme of the experimental setup is displayed in Fig. 2. The optical source for the current injection experiments is a commercial femtosecond Er:fiber laser (Toptica FFS). It delivers a 75 MHz pulse train of 250 mW average power and 90 fs pulse duration at a central wavelength of 1.55 μm. Such telecom radiation is well suited to induce two-photon absorption in GaAs since $2\hbar\omega=1.6$ eV $>E_G=1.42$ eV (values refer to room temperature where the experiment is conducted). The light is passed through a 2 mm BiBO nonlinear optical crystal to generate several mW of second harmonic radiation at 775 nm. A phase-stable superposition of copolarized fundamental (ω) and second-harmonic radiation (2ω) is synthesized in a two-color Michelson interferometer utilizing a dichroic beamsplitter. A high-precision motorized stage and polarization optics ensure full control over the relative phase and the polarization state of the $\omega/2\omega$ pulse pair. The light is focused onto the sample using an aspheric lens with a numerical aperture of NA = 0.26. Spot sizes are $\approx(10\ \mu\text{m})^2$ for ω radiation and 20 μm × 35 μm for 2ω light (note that

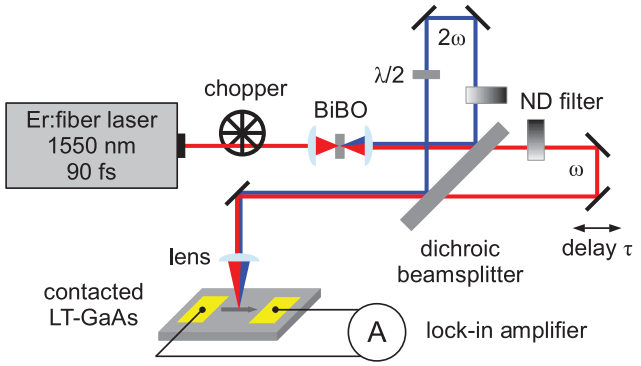

FIG. 2. (Color online) Schematic of the experimental setup: An Er:fiber laser generates 1.55 μm femtosecond pulses that are partially frequency doubled in a BiBO crystal. The individual intensity, the relative delay τ, and the polarization of the fundamental and the second harmonic can be controlled in a two-color interferometer. Both beams are focused on a contacted LT-GaAs sample; the photoinduced potential difference between the contacts is measured with a lock-in amplifier.

slightly different spot sizes are linked to the second-harmonic generation and the chromatic aberration of the focusing optics). The photocurrent is extracted with a lock-in amplifier referenced to the exciting light that is mechanically chopped at 570 Hz. For the experiments presented in Sec. IV C, we add a third interferometer arm into the setup. It allows for additional pumping of the semiconductor specimen with ω excitation with a variable timing with respect to the $\omega/2\omega$ pulse pair injecting the current.

The sample is based on a nominally undoped, annealed 2 μm thick low temperature grown (LT-)GaAs epilayer on an intrinsic GaAs substrate. This material has proven well suited for efficient injection and electrical detection of coherently controlled photocurrents.[5,15] The most favorable aspect of this material is the possibility to characterize coherently controlled currents by metallic electrodes in the vicinity of the excitation. In essence, the short lifetime of unbound electrons in LT-GaAs inhibits dielectric charge relaxation and leads to a long-lived in plane electrical dipole which manifests as a voltage drop between adjacent metal pads.[5,15] We note that we have measured the lifetime of the unbound electron-hole pairs by time-resolving the free-carrier absorption subsequent to photoexcitation. For the sample of this study, we find a lifetime of 1–2 ps, consistent with previous reports.[16,17]

On the LT-GaAs specimen, gold electrodes with a gap of 50 μm are formed by optical lithography. Coherently controlled currents can be generated and electrically measured in the LT-GaAs substrate throughout the entire gap between the gold electrodes. Due to differing detection efficiencies, the magnitude of the phase-dependent signal in the external circuit varies with the distance between the excitation position and the electrodes as found before.[15] A phase-independent photocurrent offset reflects photoresponses from the illumination outside the center of the device. As expected from the response of Schottky contacts, it is most pronounced for excitations close to the electrodes. We therefore illuminate the center of the device to reduce potential influences of the metal contacts.

Figure 3(b) shows an exemplary scan of photocurrent as a function of the relative timing within the $\omega/2\omega$ pulse pair. In contrast to theoretical models typically predicting dJ/dt, our measurement detects a current magnitude temporally integrated over the optical pulse and averaged over many excitation cycles. The data shows pronounced interferometric oscillations $\propto \sin(2\phi_\omega - \phi_{2\omega})$, i.e., a carrier wave with the wavelength of the second harmonic. This phase dependence is consistent with the established picture of current injection.[4–6] The amplitude of the oscillatory signal reveals the magnitude of the coherently controlled photocurrent. However, the actual in plane-current is probably larger since no effort is made to optimize the charge extraction to the contacts. We also note that even current magnitudes as small as ~500 pA evidence substantial μA in-plane peak currents, since current bursts of sub-picosecond duration are injected every 13 ns and we measure time-averaged quantities. For most of the discussion below, we analyze the peak amplitude of the interferometric signal as a function of the $\omega/2\omega$ irradiance (note that these signal strengths will be referred to as coherently controlled currents in the remainder of the manuscript even though the actual values will differ because of the imperfect charge extraction to the contacts and the intrinsic pulsed character of coherently controlled currents). However, for some aspects presented in Sec. IV it proves advantageous to also consider the entire τ dependence of the photocurrent.

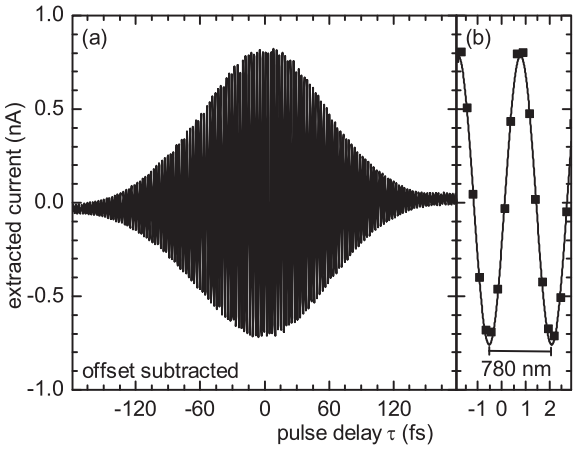

FIG. 3. (a) Current interferogram as recorded by detecting the photoresponse upon $\omega/2\omega$ irradiance as a function of the relative timing τ. A τ-independent offset is subtracted from the data. The shape corresponds to a convolution of both pulse envelopes modulated with a sine wave at a wavelength of the 2ω light. (b) The closeup around $\tau = 0$ reveals the carrier wave.

IV. EXPERIMENTAL RESULTS

This section contains the central experimental results of the paper. We start with an analysis of the magnitude of the coherently controlled current as a function of the $\omega/2\omega$ irradiance (cf. Sec. IV A). Since those data do potentially not only reflect the photoinduced current strengths but are also influenced by the relaxation dynamics of the photoinduced electron-hole dipole, we offer additional time-resolved experiments to produce a consistent overall picture of photocurrent generation, absorption saturation, and carrier relaxation dynamics. In particular, in Sec. IV B we directly confirm the absorption saturation during the ultrafast light-matter interaction. Then we elucidate the dynamics and the diagnostics of the photoinduced electric dipole in Sec. IV C. Finally, signatures of saturation effects on the temporal shape of the current interferograms will be presented in Sec. IV D.

A. Irradiance dependence of the coherently controlled currents

Figure 4 displays the magnitude of the injected current for numerous combinations of the field strengths E_ω and $E_{2\omega}$. The electric fields represent the peak field amplitudes of the pulses within the GaAs sample deduced from the incident optical intensity corrected for reflection losses. For comparison, the upper abscissa of Fig. 4 also contains information about the corresponding irradiance levels. The values for the current strengths are determined from the amplitude of the oscillatory signal during optimal $\omega/2\omega$ overlap (cf. the exemplary traces in Fig. 3). For all the $E_{2\omega}$ irradiances used for Fig. 4 we observe a quadratic rise of the coherently controlled current as a function of a moderate field E_ω. This is consistent with the perturbative picture of coherent control whereby

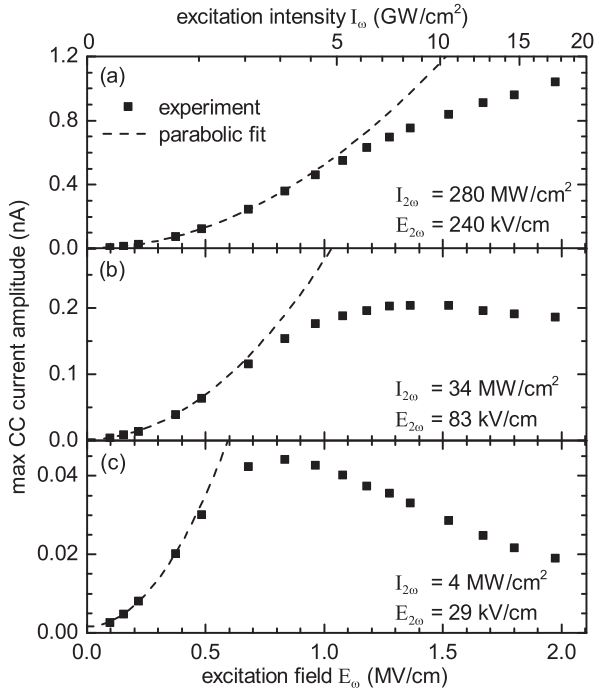

FIG. 4. Amplitude of the phase-dependent photoresponse for various combinations of illumination strengths I_ω and $I_{2\omega}$. The data represent amplitudes of the sinusoidal signals at $\tau \approx 0$ as seen in Fig. 3(b). The dashed lines are quadratic dependencies which correspond to the perturbative $\chi^{(3)}$ model.

$dJ/dt \propto E_\omega^2 E_{2\omega}$ is expected. More interestingly, marked departures from this prediction are seen for field strength $E_\omega \geqslant 0.5$ MV/cm. Those saturation effects occur at very similar $\omega/2\omega$ excitation strengths as predicted from the simulation results shown in Fig. 1. In particular, the E_ω dependence seen in Fig. 4(a) matches the theoretical results for $E_{2\omega} = 180$ kV/cm in Fig. 1 very well. For moderate $E_{2\omega}$ illumination [cf. Fig. 4(c)] the saturation effects in the experiment are more pronounced when compared to the theoretical expectation. Ultimately, even a pronounced decrease of the current as a function of the ω field strength is visible in Fig. 4(c). As further corroborated by experiments shown in Sec. IV C, the current reduction in Fig. 4(c) is mainly driven by internal discharge effects due to the elevated carrier density generated by ω irradiance.

We also note that we have additionally analyzed current injection with perpendicularly polarized ω and 2ω pulses. In such a configuration, current injection takes advantage of the element η_{xyyx} of the current injection tensor. This tensor describes the relation of the current injection rate to the driving electrical fields and is directly linked to the imaginary part of $\chi^{(3)}(0,\omega,\omega,-2\omega)$.[4] η_{xyyx} is much smaller when compared to the element η_{xxxx} and gives rise to a current in the direction of the 2ω polarization. In the experiment, the observed phase-dependent photoresponses are indeed markedly reduced to the values seen in Fig. 4. However, the current saturation looks very similar to the above results for parallel $\omega/2\omega$ polarizations (data not shown). In addition, we observe increased current magnitudes but similar saturation effects in a sample with a gap of 25 μm between the gold electrodes. Taken together, the saturation effects are therefore actually linked to the optical irradiance levels as opposed to potential saturation effects in the charge extraction.

It is also interesting to compare the results from Fig. 4 with the general expectations for higher order optical nonlinearities in GaAs. Current injection is usually attributed to the imaginary part of $\chi^3(0,\omega,\omega,-2\omega)$. In a Taylor expansion of the nonlinear optical polarization, any saturation effect seen for elevated ω irradiance can be interpreted as arising from a fifth-order term $\chi^5(0,\omega,\omega,\omega,-\omega,-2\omega)$. For the field strengths $E_\omega = 2.0$ MV/cm and $E_{2\omega} = 240$ kV/cm [cf. Fig. 4(a)], this correction term leads to an injected current 50% smaller than predicted by the $\chi^{(3)}$ scaling. This consideration gives rise to an estimate of $\mathrm{Im}\chi^5(0,\omega,\omega,\omega,-\omega,-2\omega)/\mathrm{Im}\chi^3(0,\omega,\omega,-2\omega) \approx 1 \times 10^{-13}$ cm^2/V^2, consistent with an estimate based on scaling laws for multiphoton absorptions.[18,19]

We now want to comment about the direct comparability of the simulation results in Sec. II to the present experimental findings. First of all, a comparison of the absolute current magnitudes is beyond the scope of the study because the experimental values, e.g., depend on the location of the excitation spot on the metal-semiconductor-metal microstructure as well as the unknown efficiency of charge extraction into the contacts. The simulation takes into account a realistic description of the band structure of GaAs and an appropriate interaction of one- and two-photon absorption processes. However, the experiment is likely influenced by two additional factors: (i) We work with Gaussian pulse envelopes in time and space whereas the simulation only considers plane waves with the temporal profile of the experiment. (ii) The experiments utilizes LT-GaAs samples because its large defect density inhibits dielectric charge relaxation and leads to a long-lived in plane electrical dipole which we in turn measure as a voltage drop between adjacent metal pads. The simulation, however, does only treat the current injection itself in pure GaAs and does not account for the charge accumulation and dipole relaxation.

The defect states in LT-GaAs provide an additional absorption path for ω excitation. From conventional infrared spectroscopy we learn that the respective absorption coefficient in our LT-GaAs specimen is $\alpha_\omega \approx 750$ cm^{-1} which probably corresponds to a defect density in the order of 10^{18} cm^{-3}.[20,21] From z-scan measurements we know that the two-photon-absorption coefficient for GaAs is $\beta = 3.5$ cm/GW—comparable to previous studies.[22] For an excitation intensity of $I_\omega = 15$ GW/cm^2 those quantities give rise to a carrier density of 5×10^{17} cm^{-3} for two-photon absorption and up to 8×10^{18} cm^{-3} for the absorption of deep defect states. The latter quantity, however, can only be seen as an upper bound because it is comparable to the overall density of defects. We also note that the excitation of defect states involves final states in the conduction band different from those of the interband photon absorption.[21,23]

The generated carriers lead to a substantial blocking of the final states. Furthermore, the elevated carrier density might play an important role in discharge effects of the coherently controlled electron-hole dipole. Such discharge effects are not contained in the simulation in Sec. II. Taken together, the qualitative agreement between the theoretical results in Fig. 1 and the experimental results in Fig. 4

are an important hint for departures from the perturbative picture of current injection. However, in the following we will present several additional experiments to confirm that many aspects of the observed current saturation are indeed linked to macroscopic states filling during the ultrafast light-matter interaction.

B. Absorption saturation in GaAs

As a first step, we perform optical pump-probe experiments to confirm that the ω irradiance of our experiment indeed leads to substantial state filling via two-photon absorption. To rule out any influence of the deep defects of LT-GaAs, this part of the study is done with an intrinsic GaAs thin film of 400 nm thickness. For an intensity of $I_\omega = 7.5$ GW/cm^2 and a 775 nm (2ω) probe, we detect a transient increase of the probe transmission as large as 1.6% that relaxes with time constants of 100 fs and 2 ps, related to electron thermalization via carrier-carrier scattering and electron-phonon interaction. A comparison of the signal strength with previous pump-probe experiments in clean GaAs[24] points towards two-photon induced carrier densities of 2×10^{17} cm^{-3}. As a result, the two-photon absorption responsible for current injection leads to substantial final state blocking. Also the 2ω field strengths of our study gives rise to such strong excitation regimes. As an example, if one assumes a 90 fs pulse of a field strength of $I_{2\omega} = 280$ MW/cm^2 and an absorption coefficient of $\alpha = 15\,000$ cm^{-1} typical for 775 nm light, the photoinduced carrier density would be 1.5×10^{18} cm^{-3}. We note that these excitation conditions are similar to the one found sufficient to drive interband Rabi oscillations in the similar semiconductor InP.[25] Taken together, our coherent control study therefore certainly explores strong excitation conditions that are appropriate to reveal departures from the perturbative regime.

C. Photoinduced discharge of the coherently controlled electron-hole dipole

The illumination of a semiconductor specimen with phase-related $\omega/2\omega$ pulse pairs leads to the generation of an instantaneous current which decays on sub-picosecond time scales governed by the momentum relaxation of charge carriers. After the interaction with the light field, therefore, an electron-hole dipole is present in the medium. From optical measurements in GaAs bulk and quantum well samples, the average electron-hole displacement is determined to be 20 nm to 100 nm depending on the temperature and the irradiance conditions.[26,27] For intrinsic clean GaAs samples, the decay time of the photoinduced electron-hole dipole is found to be in the order of 1 ps.[27] This ultrashort time scale originates from the dielectric relaxation due to the internal electric field and can be explained by a rigid shift model of slightly displaced electron and hole sheet distributions.[27] For the LT-GaAs material of the present study, instead, unbound electrons and holes are captured into deep defect levels within similar time scales. As a result, a long-lived in plane electrical dipole remains in the medium which manifests as a voltage drop between adjacent metal pads.[5,15] However, if one attempts to compare largely different irradiances for coherent control as

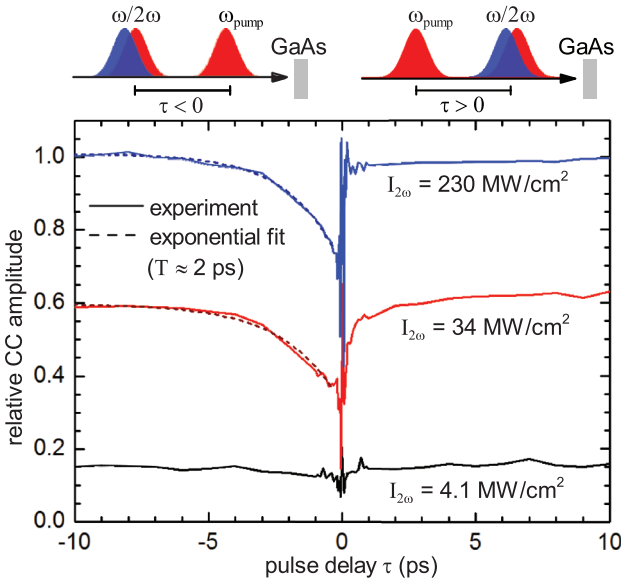

FIG. 5. (Color online) Maximum amplitude of the coherently controlled current plotted vs the delay of an additional ω pump pulse for $I_\omega^{\text{pump}} = 10$ GW/cm^2, $I_\omega = 1$ GW/cm^2 and three different $I_{2\omega}$. The signal amplitudes are normalized to the respective values observed without the pump pulse. At negative delay times the additional pump pulse impinges before the arrival of the $\omega/2\omega$ pulse pair that induces the current.

we have done in Sec. IV A, also the dipole relaxation probably changes in addition to modified photoinduced electron-hole dipole.

This question motivates the following set of experiments where we analyze the coherently controlled photoresponse of the metal-GaAs-metal structure under the influence of an additional pump pulse generating unbound charge carriers. The results are summarized in Fig. 5. It displays the maximum amplitude of the coherently controlled current observed for a relative $\omega/2\omega$ timing $\tau \approx 0$ for irradiances of $I_\omega = 1$ GW/cm^2 and three different $I_{2\omega}$ given in the graph. In addition, another portion of the ω light with a peak power of $I_\omega^{\text{pump}} = 10$ GW/cm^2 is incident on the sample before (negative time axis) or after (positive time axis) those two pulses generating the current. The pump pulse generates a carrier density of 5×10^{18} cm^{-3} via two-photon absorption and excitation of defect states. All the values for the amplitude of the coherently controlled current are normalized to the respective value detected without the influence of the additional pump light.

We start the discussion by considering the lower (black) curve in Fig. 5 where the pump induces a substantially larger carrier density when compared to the combined absorption associated with the $\omega/2\omega$ pulse pair. Most strikingly, the additional carriers injected by the pump reduce the signature of the coherently controlled current by a factor of $\sim$6 almost irrespective of the timing of the pump. Apparently, the additional carriers lead to an efficient discharge mechanism for the coherently controlled dipole. The lifetime of the electron-hole dipole is determined by the *RC* time constant of the device. Due to the large resistivity of LT-GaAs, it is probably larger than the pulse separation of 13 ns. Consequently, the dipole can be regarded as steady so that a certain pump pulse can

imply a discharge of the dipole irrespective of its timing. Such discharge effects explain the reduction of the amplitude of the coherently controlled photoresponse in Fig. 4(c) and are also consistent with previous studies reporting on signal reductions in similar devices.[8,9]

We now turn towards the upper (blue) curve in Fig. 5 where the additional pump pulse generates an electron-hole density smaller than generated by the $\omega/2\omega$ pulse pair. In this case, a marked influence of the pump-induced carriers on the observed coherently controlled photoresponse is only seen for slightly negative delay times. For such a pulse sequence, the pump pulse massively populates valence and conduction band states which, in turn, reduces the absorption and related current injection induced by the $\omega/2\omega$ pulse pair. The lifetime of this signal reduction is $\sim$2 ps which can be interpreted as a capture time of charge carriers into deep defect levels of LT-GaAs. In contrast, a pump generating unbound carriers right after the injection of a coherently controlled current (cf. slightly positive delays in Fig. 5) does not reduce the phase-dependent photoresponse (note that the data very close to zero pulse delay widely scatter due to interference of the two simultaneous pulses with central frequency ω). As a result, the signatures of coherently controlled currents for elevated 2ω peak powers [cf. Fig. 4(a) and the upper (blue) curve in Fig. 5] are not strongly influenced by discharge effects. The results of Fig. 5, therefore, are indicative of substantial band filling by the irradiance conditions of the study.

D. Temporal shape of the current interferograms

Due to the finite pulse lengths the strong dependence on the temporal ordering of the ω and 2ω pulses should also manifest as asymmetries in the current interferograms such as the one shown in Fig. 3(a). These asymmetries should give insight into the short-time behavior of the saturation that is concealed by interference artifacts in the previous measurements. Therefore we have recorded current interferograms for various combinations of ω and 2ω irradiances in the two-arm setup. Figure 6(a) shows the temporal envelopes of such interferograms for a fixed $I_{2\omega} = 340$ MW/cm^2 and three different ω peak powers. Note that the time-independent saturation cancels out as all envelopes have been normalized to their respective maximum. Furthermore, the reproducibility of the delay stage in the interferometer is 50 nm and, therefore, reliably allows us to trace minute changes of the temporal profiles of the interferograms. The most pronounced modifications occur for $\tau < 0$ where the ω pulse precedes the 2ω. In such a configuration, two-photon absorption and excitation of defect states by the fundamental radiation already induce substantial band filling.

For a more quantitative analysis, we have extracted the temporal width (FWHM) of the interferograms' envelopes that is independent of the normalization. The result is depicted in Fig. 6(b). With increasing peak intensity I_ω, we find the temporal width to decrease by about 10% for all three 2ω illumination levels shown. The reduction of the temporal width arises mainly from a signal reduction at the slope at $\tau < 0$. In such a configuration, elevated ω irradiances block final states for the interband absorption such that the current is reduced with respect to the $\chi^{(3)}$ expectation.

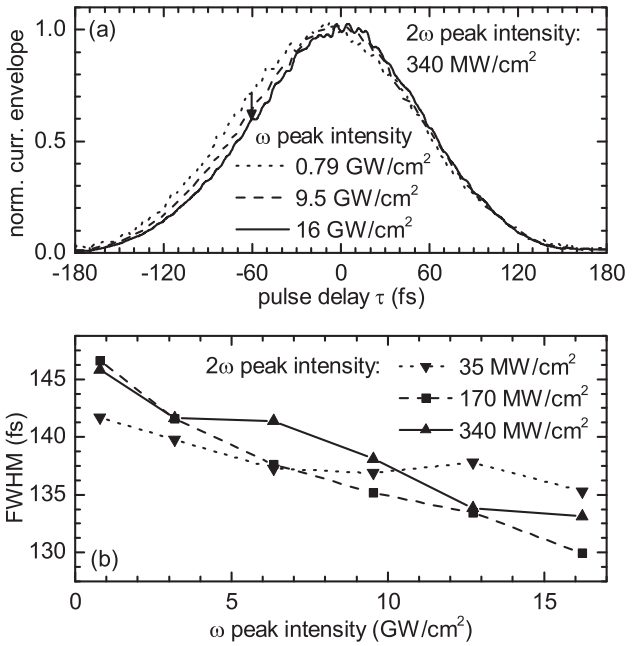

FIG. 6. (a) Maximum amplitude of the coherently controlled current as a function of the relative timing τ of the harmonically related spectral components. The curves represent the normalized difference of the upper and lower envelopes of current interferogram such as displayed in Fig. 3(a). The different lines correspond to different ω peak intensities. Negative delays $\tau < 0$ indicate an arrival of the ω pulse before the 2ω pulse. The arrow at $\tau = -60$ fs illustrates the signal reduction. (b) Temporal width (FWHM) of the envelopes plotted for various combinations of ω and 2ω peak irradiances.

Taken together, the additional τ-dependent data confirm that the saturation affects seen for elevated $\omega/2\omega$ power levels indeed reveal new insight into deviations of the current injection process beyond the perturbative limit. The results directly evidence that the scaling behavior $dJ/dt \propto E_\omega^2 E_{2\omega} \sin(2\phi_\omega - \phi_{2\omega})$ only holds true in the weak-irradiance limit while deviations for stronger excitation are necessary to fully explain the interferograms' envelopes seen in Fig. 6(a).

V. CONCLUSION

In conclusion, we have identified marked departures from the perturbative $\chi^{(3)}$ expectation of $\omega/2\omega$ current injection in bulk GaAs in both theory and experiment. They are directly linked to macroscopic state filling during the ultrafast light-matter interaction and lead to a significant current reduction at elevated irradiances. The results are of particular importance for a quantitative understanding of current injection in nanoscale devices where tightly focused femtosecond pulses easily reach the irradiances of the present study.

ACKNOWLEDGMENTS

We thank D. Schuh and W. Wegscheider for providing the LT-GaAs material and S. Thunich and A. W. Holleitner for the microstrucure fabrication. This work is supported by the DFG in the frameworks of the priority program SPP 1391 "Ultrafast Nanooptics," the project ME 1916/2, and the research training group GRK 1464.

*Corresponding author: markus.betz@tu-dortmund.de

[1]E. L. Ivchenko and G. E. Pikus, *Superlattices and Other Heterostructures: Symmetry and Optical Phenomena* (Springer, Berlin, 1997).

[2]S. D. Ganichev, E. L. Ivchenko, V. V. Belkov, S. A. Tarasenko, M. Sollinger, D. Weiss, W. Wegscheider, and W. Prettl, Nature (London) **417**, 153 (2002).

[3]D. Côté, N. Laman, and H. M. van Driel, Appl. Phys. Lett. **80**, 905 (2002).

[4]R. Atanasov, A. Haché, J. L. P. Hughes, H. M. van Driel, and J. E. Sipe, Phys. Rev. Lett. **76**, 1703 (1996).

[5]A. Haché, Y. Kostoulas, R. Atanasov, J. L. P. Hughes, J. E. Sipe, and H. M. van Driel, Phys. Rev. Lett. **78**, 306 (1997).

[6]L. Costa, M. Betz, M. Spasenović, A. D. Bristow, and H. M. van Driel, Nat. Phys. **3**, 632 (2007).

[7]C. Ruppert, S. Thunich, G. Abstreiter, A. Fontcuberta i Morral, A. W. Holleitner, and M. Betz, Nano Lett. **10**, 1799 (2010).

[8]D. Côté, J. M. Fraser, M. DeCamp, P. H. Bucksbaum, and H. M. van Driel, Appl. Phys. Lett. **75**, 3959 (1999).

[9]A. Haché, J. E. Sipe, and H. M. van Driel, IEEE J. Quantum Electron. **34**, 1144 (1998).

[10]B. A. Ruzicka and H. Zhao, Phys. Rev. B **79**, 155204 (2009).

[11]H. T. Duc, T. Meier, and S. W. Koch, Phys. Rev. Lett. **95**, 086606 (2005).

[12]H. T. Duc, Q. T. Vu, T. Meier, H. Haug, and S. W. Koch, Phys. Rev. B **74**, 165328 (2006).

[13]B. Pasenow, H. T. Duc, T. Meier, and S. W. Koch, Solid State Commun. **145**, 61 (2008).

[14]R. Winkler, *Spin-Orbit Coupling Effects in Two-Dimensional Electron and Hole Systems* (Springer, Berlin, 2003).

[15]P. Roos, Q. Quraishi, S. Cundiff, R. Bhat, and J. E. Sipe, Opt. Express **11**, 2081 (2003).

[16]P. Grenier and J. F. Whitaker, Appl. Phys. Lett. **70**, 1998 (1997).

[17]T. S. Sosnowski, T. B. Norris, H. H. Wang, P. Greiner, J. F. Whitaker, and C. Y. Sung, Appl. Phys. Lett. **70**, 3245 (1997).

[18]J. M. Fraser and H. M. van Driel, Phys. Rev. B **68**, 085208 (2003).

[19]B. S. Wherrett, J. Opt. Soc. Am. B **1**, 67 (1984).

[20]S. U. Dankowski, P. Kiesel, B. Knüpfer, M. Kneissl, G. H. Döhler, U. D. Keil, D. R. Dykaar, and R. F. Kopf, Appl. Phys. Lett. **65**, 3269 (1994).

[21]M. O. Manasreh, D. C. Look, K. R. Evans, and C. E. Stutz, Phys. Rev. B **41**, 10272 (1990).

[22]W. C. Hurlbut, Y.-S. Lee, K. L. Vodopyanov, P. S. Kuo, and M. M. Fejer, Opt. Lett. **32**, 668 (2007).

[23]D. C. Look, Thin Solid Films **231**, 61 (1993).

[24]R. Tommasi, P. Langot, and F. Vallée, Appl. Phys. Lett. **66**, 1361 (1995).

[25]C. Fürst, A. Leitenstorfer, A. Nutsch, G. Tränkle, and A. Zrenner, Phys. Status Solidi B **204**, 20 (1997).

[26]H. Zhao, A. L. Smirl, and H. M. van Driel, Phys. Rev. B **75**, 075305 (2007).

[27]H. Zhao, E. J. Loren, A. L. Smirl, and H. M. van Driel, J. Appl. Phys. **103**, 053510 (2008).